How to cite: Angew. Chem. Int. Ed. 2024, e202407038
doi.org/10.1002/anie.202407038

Urea Oxidation | Hot Paper

Regulating Reconstruction-Engineered Active Sites for Accelerated Electrocatalytic Conversion of Urea

Jichao Zhang[+], Jianrui Feng[+], Jiexin Zhu[+], Liqun Kang, Longxiang Liu, Fei Guo, Jing Li, Kaiqi Li, Jie Chen, Wei Zong, Mingqiang Liu, Ruwei Chen, Ivan P. Parkin, Liqiang Mai,* and Guanjie He**

Abstract: Reconstruction-engineered electrocatalysts with enriched high active Ni species for urea oxidation reaction (UOR) have recently become promising candidates for energy conversion. However, to inhibit the over-oxidation of urea brought by the high valence state of Ni, tremendous efforts are devoted to obtaining low-value products of nitrogen gas to avoid toxic nitrite formation, undesirably causing inefficient utilization of the nitrogen cycle. Herein, we proposed a mediation engineering strategy to significantly boost high-value nitrite formation to help close a loop for the employment of a nitrogen economy. Specifically, platinum-loaded nickel phosphides (Pt-Ni_2P) catalysts exhibit a promising nitrite production rate (0.82 mol kWh^{-1} cm^{-2}), high stability over 66 h of Zn-urea-air battery operation, and 135 h of co-production of nitrite and hydrogen under 200 mA cm^{-2} in a zero-gap membrane electrode assembly (MEA) system. The in situ spectroscopic characterizations and computational calculations demonstrated that the urea oxidation kinetics is facilitated by enriched dynamic Ni^{3+} active sites, thus augmenting the "cyanate" UOR pathway. The C–N cleavage was further verified as the rate-determining step for nitrite generation.

Introduction

The electrochemical oxidation of small molecules (methanol, ethanol, hydrazine, and urea, etc.), with significantly lower thermodynamic potential, exhibits promising routes to replace the oxygen evolution reaction (OER) in various energy conversion applications.[1–3] Among those small molecule reactants, urea (non-toxicity and non-flammability), can be easily accessed from domestic wastewater (e.g. human urine). Nickel-based catalysts have been extensively reported due to the highly active dynamic Ni^{3+} active sites for UOR.[4,5] However, the mechanism of the UOR remains debated. Two main pathways, involving the "carbonate" pathway ($CO(NH_2)_2+8OH^-\rightarrow CO_3^{2-}+N_2+6H_2O+6e^-$) and "cyanate" pathway ($CO(NH_2)_2+8OH^-\rightarrow NCO^-+NO_2^-+6H_2O+6e^-$), have been extensively investigated.[6] Viktoriia et al. proposed a potential-dependent relationship between those two pathways and enriched NiOOH species at high potentials could lead to the dominating role of the "cyanate" pathway with toxic nitrite formation.[7] Accordingly, complicated and high-cost strategies were implemented to improve the selectivity of innocuous nitrogen gas (N_2) to avoid over-oxidation, pointlessly generating a lot of low economic value of N_2.[6,8]

Despite the concern of toxicity for nitrite, it plays a vital role in industrial areas, such as pharmaceuticals, agriculture, and food processing.[9,10] Moreover, the bottleneck of NO_x electro-reduction is still limited by the low natural feedstock for large-scale electrosynthesis of NH_3 with high concentration.[11] Provided that we produce the high-value nitrite directly from adequate urea-bearing wastewater (e.g. mammalian urine) to offer an oxidized form of N, a closed loop of environmentally-friendly nitrogen supply chains would be constructed, realizing a sustainable nitrogen

[*] J. Zhang,[+] J. Feng,[+] F. Guo, K. Li, J. Chen, W. Zong, M. Liu, R. Chen, I. P. Parkin, G. He
Christopher Ingold Laboratory, Department of Chemistry, University College London (UCL), 20 Gordon Street, London WC1H 0AJ, UK
E-mail: g.he@ucl.ac.uk
i.p.parkin@ucl.ac.uk

J. Zhu,[+] L. Mai
State Key Laboratory of Advanced Technology for Materials Synthesis and Processing, Wuhan University of Technology, Wuhan Hubei 430070, China
E-mail: mlq518@whut.edu.cn

L. Kang
Department of Inorganic Spectroscopy, Max-Planck-Institute for Chemical Energy Conversion, Stiftstr. 34–36, 45470 Mülheim an der Ruhr, Germany

L. Liu
Department of Materials, University of Oxford, Parks Road, Oxford OX1 3PH

J. Li
Materials Research Institute, School of Engineering and Materials Science, Faculty of Science and Engineering, Queen Mary University of London, Mile End Road, London E1 4NS, UK

[+] J. C. Z, J. R. F, and J. X. Z contributed equally to this work.

economy, and simultaneously reducing the risk to the ecological environment.

As revealed by numerous studies, over 50 % conversion from urea to nitrite (NO_2^-) could be achieved by nickel oxide/hydroxide, particularly at high potentials.[12] However, the strong dependence on the applied potential to generate abundant high-active NiOOH species is not desirable for energy-saving vision. As compared to widely-used nickel oxide/hydroxide catalysts, nickel phosphides, sulfides, and nitrides exhibit good metallic electrical conductivity to facilitate electron transfer.[13–15] Notably, the stronger nucleophilicity of the in situ formed phosphate species (HPO_4 $pK_a = 12.7$, HSO_4 $pK_a = 1.99$, HNO_3 $pK_a = -1.3$) during the surface reconstruction makes it possible to facilitate the adsorption and dehydrogenation of urea molecules.[16] Nonetheless, the surface reconstruction of nickel phosphides to in situ generate more NiOOH species has been hindered by the electro-repulsion between phosphate and hydroxide anion, which has been recently ascertained by Qiao's group.[13] Furthermore, as revealed by our previous studies,[17,18] due to the insufficient Ni^{3+} active sites, the competition issue between UOR and OER is another enormous challenge to overcome (Figure 1a).[17,19,20]

Metal mediation engineering strategies have been considered an effective route to modulate the proton-coupled-electron-transfer (PCET) process.[21] Despite the enormous efforts to develop the non-noble metal mediation method, Platinum (Pt) still possesses a higher activity and ultra-stable durability in numerous energy conversion systems.[22] Pt with partially filled 5d orbitals creates the possibility of interacting with various molecules, enabling fast electron transfer around the reaction microenvironments.[23] Motivated by the tuning ability of adsorption/desorption for reactants and intermediates from Pt sites, we herein proposed a Pt-mediated strategy to facilitate the OH^- adsorption and optimize the electron distribution around Pt–Ni sites, thus generating abundant dynamic Ni^{3+} active sites during surface reconstruction of nickel phosphides. Combined with in situ spectroscopic investigation and DFT calculations, it is disclosed that the notable enriched Ni^{3+} active species would accelerate urea conversion mainly according to the "cyanate" pathway for high-value nitrite formation (Figure 1b). More CNO^- species were detected, demonstrating rapid C–N bond cleavage during the UOR process. Besides, Incorporating Pt sites could significantly lower the energy barrier for C–N bond cleavage, which was found as the rate-determining step to generate high-value nitrite products. This facile and feasible mediation strategy opens a unique avenue to fix issues during UOR and is anticipated to be extended to other energy conversion scenarios.

Results

Catalyst Synthesis and Electrochemical Performance Analysis

The Pt was first incorporated on nickel phosphide catalysts based on nickel foams via solution reduction synthesis. A single phase of Ni_2P (PDF No. 89-4864) was revealed by the X-ray diffraction (XRD) patterns (Supplementary Figure S1a). The high-resolution transmission electron microscopy (HRTEM) image presents Pt nanoparticles with (111) lattice, indicating successful construction of Pt sites on Ni_2P catalysts (Supplementary Figure S1b). The corresponding energy dispersive spectroscopy (EDS) line scanning and mapping images further indicate the uniform distribution of Pt on the Ni_2P catalyst. The different feed amounts of Pt precursors were also investigated by microwave plasma atomic emission spectrometers (MP-AES), with the loading mass of 20, 80, and 131 $\mu g\,cm^{-2}$ when utilizing 20, 50, and 150 μL Pt precursors (Sary Figure 2a). According to the results of XRD patterns and scanning electron microscope (SEM) images, the Pt was incorporated into Ni_2P catalysts with a notable change in the roughness of morphologies (Supplementary Figure S2b and S3), offering a strong possibility of optimizing the interaction between reactants/intermediates with electrode surface.

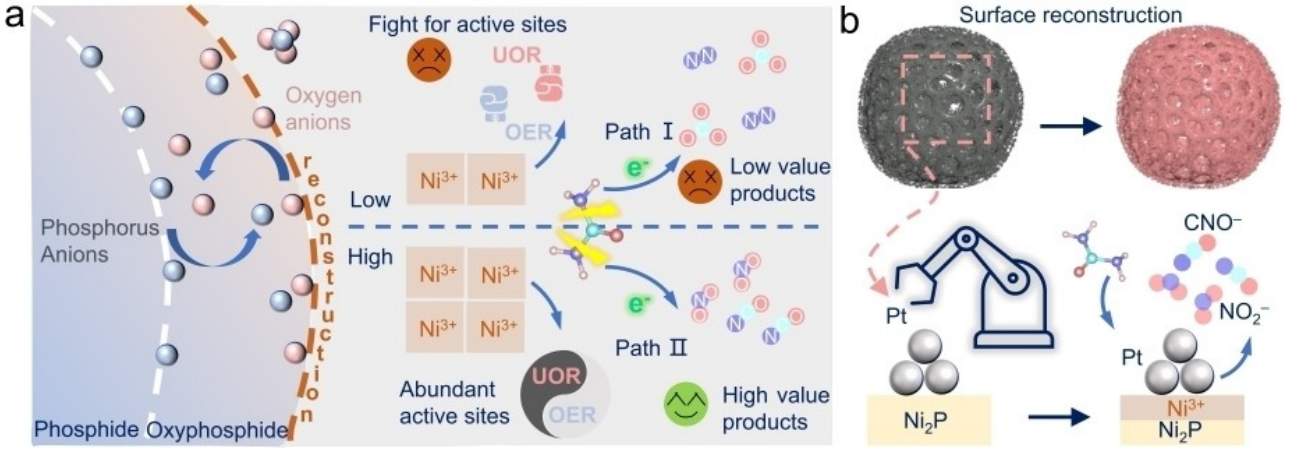

Figure 1. **Schematic illustration of current issues and our solutions. a** Issues correlated to the competition and low-value products due to insufficient active sites for reconstruction-engineered catalysts. **b** The highlight of Pt-Ni_2P catalysts.

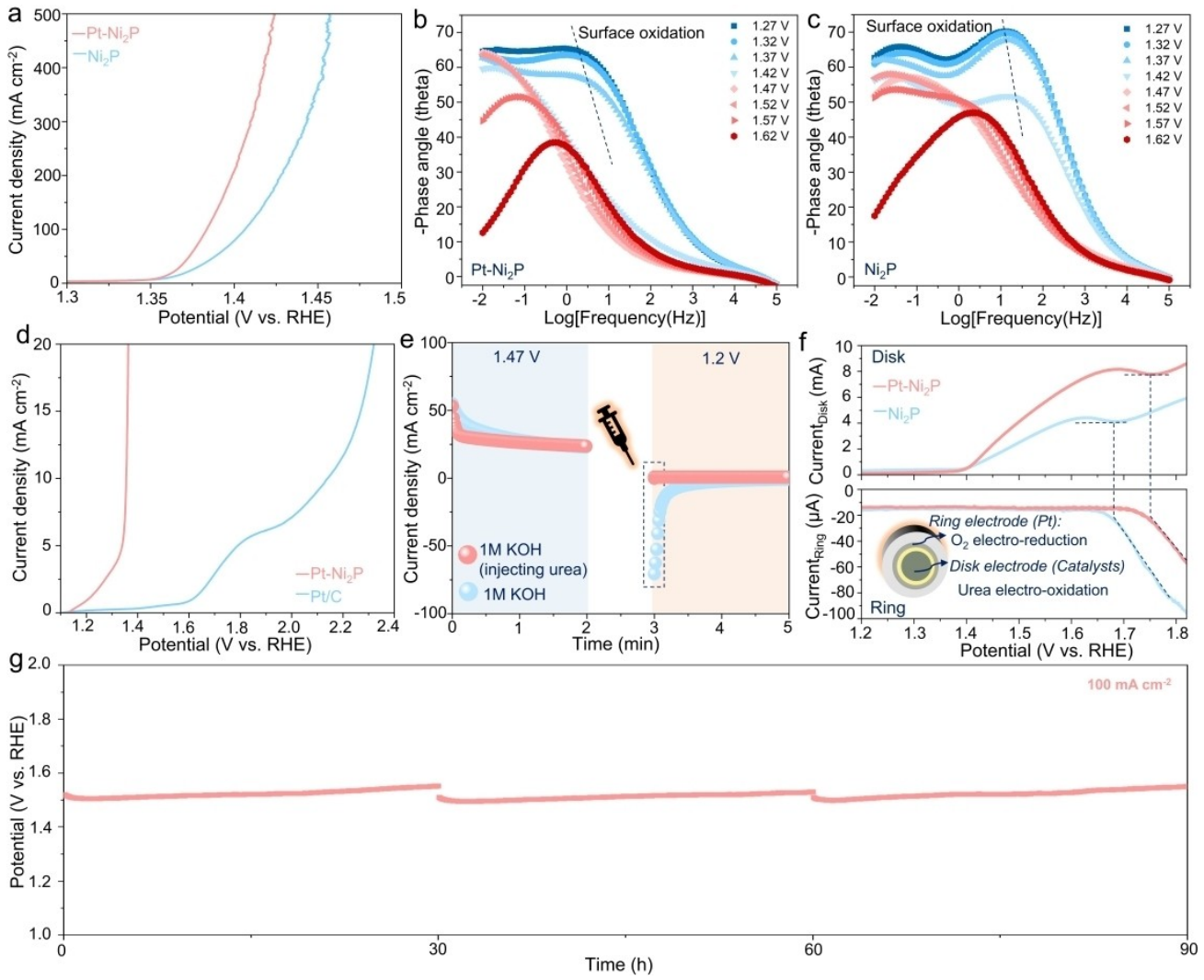

Figure 2. **2 Electrochemical performance.** **a** Polarization curves of Ni_2P and Pt-Ni_2P catalysts. **b–c** In situ EIS for OER at different potentials. **d** Polarization curves of Pt/C and Pt-Ni_2P catalysts. **e** Intermittent UOR test. **f** RRDE system (1600 rpm) for oxygen reduction detection with the applied potential bias of 0.2 V vs RHE on the ring electrode. **g** Stability test at 100 mA cm^{-2} over 90 hours (adding fresh electrolyte every 30 hours).

The electrochemical UOR performance was subsequently evaluated in a three-electrode system. The Pt-Ni_2P catalysts required only 1.38 V vs. RHE to reach the current density of 100 mA cm^{-2} (Figure 2a) and yield a remarkably smaller Tafel slope (28.3 mV dec^{-1}), implying accelerated UOR kinetics and outperform most recently reported electrocatalysts (Supplementary Figure S4a and Table S1). The potential was negatively shifted by 203 mV as compared to the OER under the current density of 100 mA cm^{-2} (Supplementary Figure S4b). The feed amounts of the Pt precursor (50 μL) were confirmed as the optimized ratio with good commercial feasibility (Supplementary Figure S4c).

The in situ electrochemical impedance spectroscopy (EIS) investigation was thereafter performed to unearth the potential-dependent interfacial charge transfer in different phases. To obviate the effect of urea dehydrogenation on the Ni^{3+} species formation, in situ EIS studies were conducted in 1 M KOH (Figure 2b and c). The peak in the Bode plot can be observed at high frequency, corresponding to the surface oxidation to form Ni^{3+} species (Supplementary Figure S5).[24–26] It is notable that the phase angle remarkably decreases when the potential reaches 1.37 V vs. RHE and disappears after 1.42 V vs. RHE, signifying the rapid formation of Ni^{3+} species on the surface. To probe the role of Pt sites in the generation of Ni^{3+} species, the Faradaic charge transfer for Ni^{2+} to Ni^{3+} was calculated (Supplementary Figure S6a and b). Introducing Pt sites remarkably boosted the Ni^{3+} active species formation with a higher Faradaic charge of 854 mC. Additionally, the reduction peak of cyclic voltammetry (CV) curves during UOR features an enhanced and negative trend than Ni_2P catalysts. This reduction peak correlated to Ni^{3+} to Ni^{2+} elucidated a higher concentration of Ni^{3+} species when incorporating Pt sites (Supplementary Figure S6c). The electrochemical double-layer capacitance (C_{dl}) can reflect the electrochemically active surface area (ECSA). The C_{dl} of Pt–Ni_2P is

11.5 mF cm^{-2}, higher than Ni_2P (Supplementary Figure S6 d–f), substantiating increased ECSA via introducing Pt sites.

The Pt/C catalyst was further utilized as the control sample to verify the activity of Pt during UOR (Figure 2d). It was discovered that the onset potential of the Pt/C catalyst was around 1.6 V vs. RHE, corroborating an undesirable activity for urea conversion with only Pt sites. To further comprehend the electrochemical process of the UOR, the intermittent UOR test was carried out by separating the process of the urea dehydrogenation and proton deintercalation from the catalyst (Figure 2e). An oxidation current related to forming NiOOH species was first observed in 1 M KOH at 1.47 V vs. RHE and lasted for 2 mins. The 0.33 M urea was then injected at the open circuit potential (OCP) and lasted for 1 min. Intriguingly, no reduction current was observed at a cathodic applied potential of 1.2 V vs. RHE. Contrastingly, a significant reduction occurred without adding urea. According to the above results, it can be speculated that the electro-generation of oxyhydroxide species would proceed during surface reconstruction and accept protons from urea to be reduced to hydroxide spontaneously, and thus without reduction current being detected.

The OER competing effect is another enormous challenge to obviate during UOR. The rotating ring-disk electrode (RRDE) system with the elimination of the mass transfer could be an effective method to measure the O_2 generation for evaluation of the selectivity. It was perceived that negligible oxygen reduction current could be observed before 1.65 V vs. RHE for both Pt-Ni_2P and Ni_2P catalysts. Impressively, the intensified OER competition on Ni_2P would be detected at 1.67 V vs. RHE. There is a ~100 mV positive shift for Pt-Ni_2P catalysts to be affected by the OER competition, demonstrating a relatively promising selectivity as compared to pure Ni_2P catalysts. Moreover, over 90 hours of chronopotentiometry test was operated at a constant current density of 100 mA cm^{-2}, verifying good stability for practical applications under industrial currents (Figure 2g).

To decipher the effect of Pt mediation on Ni_2P catalysts and establish the structure-performance relationship, mechanism studies were accordingly performed. The XRD patterns after the stability test over 90 h exhibit negligible variation with only one single phase of Ni_2P (Supplementary Figure S7). Significant P leaching was revealed by XPS spectra before and after UOR, signifying surface reconstruction proceeding during UOR (Supplementary Figure S8a). The peaks from XPS spectra of Pt 4f located at 71.3 and 74.5 eV correspond to metallic Pt,[27,28] elucidating the stable existence of Pt sites during long-term stability test (Supplementary Figure S8b). The morphology changes were then unearthed by SEM and HRTEM (Supplementary Figure S9). Nanosheet-like structures were observed on the edge of the catalysts, which might be the formation of Ni (oxy)hydroxide species as revealed by previous studies.[29] Specifically, the amorphous layer was discovered, close to the Ni_2P phase, affirming the electro-generation of amorphous Ni (oxy)hydroxides on the edge of Ni_2P catalysts during surface reconstruction.

The surface reconstruction was further dissected by in situ spectroscopic investigation. As revealed by Raman spectra, two peaks situated at 474 and 553 cm^{-1}, corresponding to Ni^{3+}–O in NiOOH species (Figure 3a),[30] emerged at 1.42 V vs. RHE, which is notably lower than that of pure Ni_2P catalysts (1.57 V vs. RHE) (Supplementary Figure S10). When the applied potential came back to OCP, the peaks of Ni^{3+}–O could not be discernible. As for OER process, the paired peaks of Ni^{3+}–O occurred after 1.37 V vs. RHE and could be maintained at OCP (Supplementary Figure S11a). Impressively, as revealed by Raman spectra, the Ni oxyhydroxides species accumulated during OER at 1.47 V vs. RHE over 600 s would be rapidly reduced when adding urea into the electrolyte at OCP (Supplementary Figure S11b), which is in line with the results of intermittent UOR test (Figure 2e).

To capture the intermediates and disclose the reaction pathway, in situ attenuated total reflection surface-enhanced IR absorption spectroscopy (ATR-SEIRAS) studies were performed during UOR. The peaks related to the adsorption vibration of the OH^- species at 3730, 3700, 3630, and 3600 cm^{-1} showcase notable adsorption of OH^- species to facilitate the surface reconstruction when loading Pt sites on Ni_2P (Figure 3b and Supplementary Figure S12).[31] The peak centered at 2168 cm^{-1}, corresponding to the CNO^- species in the solution could be found and was much more pronounced as the potential increases.[32] As compared to pure Ni_2P catalysts, the enhanced C–N bond cleavage in urea demonstrated rapid urea conversion with Pt mediation. The above findings in terms of surface chemistry, morphologies, and spectroscopic observations, validate that introducing Pt sites can remarkably enhance the OH^- species adsorption to form active Ni^{3+} species during surface reconstruction, thus improving the UOR kinetics.

Density functional theory (DFT) calculation was then carried out to certify the consistency with the experimental observations. It showed that more negative adsorption energy of OH^- species on Pt-Ni_2P surface than that of pure Ni_2P (Supplementary Figure S13), including adsorption configuration of Ni–OH (-0.99 eV) and P–OH (-0.93 eV). The charge density distribution plots of (001) surface demonstrated an intensification of nonuniform charge distributions with Pt mediation (Figure 3c and d). The charge gradient formation would significantly affect the d-band center (E_d). The density of states (DOS) of Pt–Ni_2P and Ni_2P were subsequently calculated. It was evidenced that both Pt–Ni_2P and Ni_2P exhibit metallic character with zero band gaps, indicating an easy electron transfer for the electrochemical process. The DOS near the Fermi level (E_f) mainly originates from Ni 3d states. With Pt mediation, the enhancement of d-states near the E_f would result in Ni site upshifts from −1.74 eV to −1.64 eV (Supplementary Figure S14b). It is well-known that the E_d model is a good descriptor for adsorbate-metal interaction.[33] Introducing Pt sites on Ni_2P can strengthen the interaction with the OH^- species, thus boosting the generation of active Ni^{3+} species during surface reconstruction.

Based on the above experimental studies and theoretical calculations, it could be deduced that the surface reconstruction process of Ni_2P is fast and self-terminates to form stable high valence Ni active sites. The reconstituted Ni oxy-

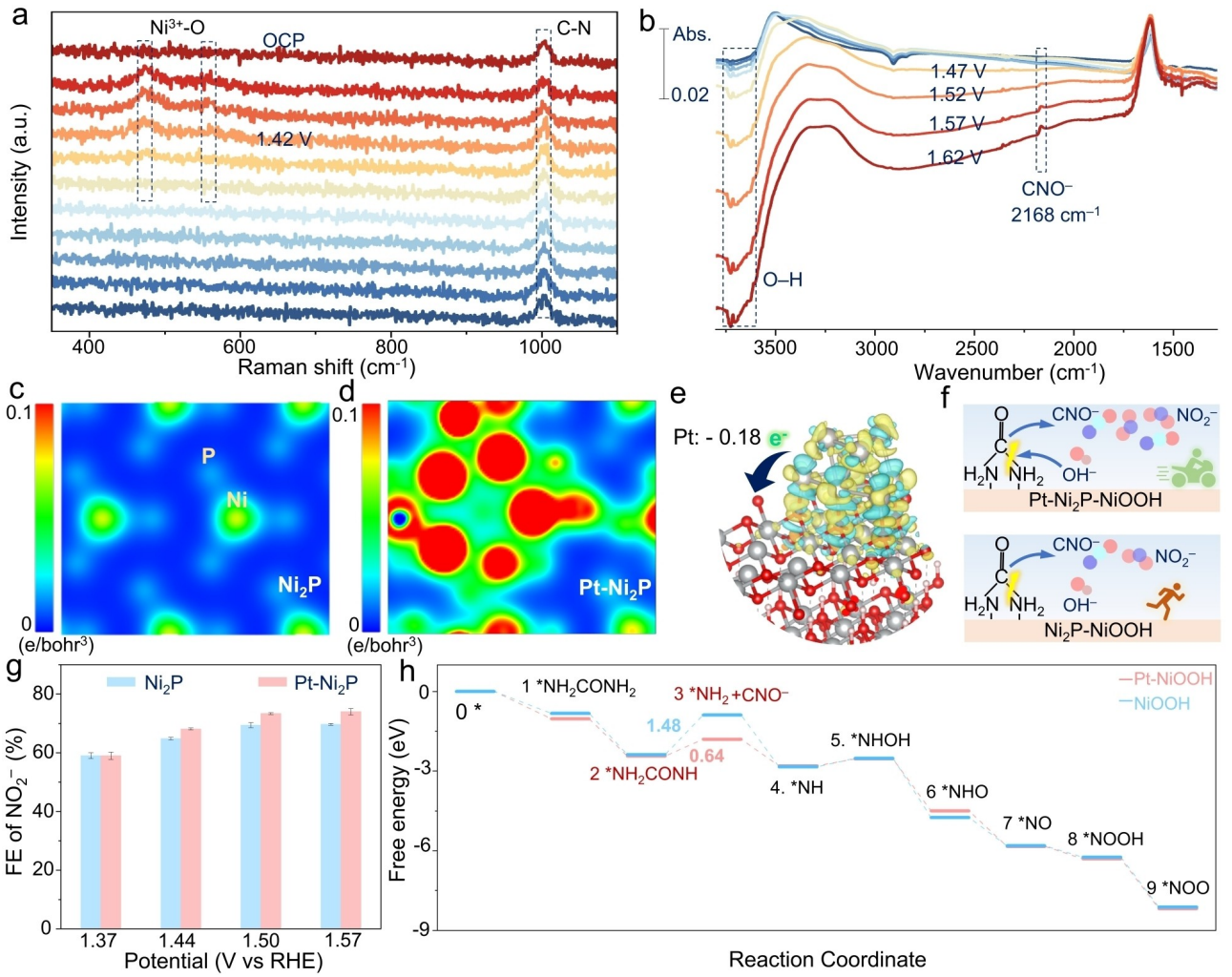

Figure 3. **Mechanism investigation during UOR. a**. Raman spectra at different applied potentials during UOR. **b** ATR-SEIRAS results at different applied potentials during UOR. **c–d** Charge density distribution plots of (001) surface for Ni_2P and Pt-Ni_2P catalysts. **e** Charge density difference of Pt-NiOOH (The blue/yellow region represents the electron accumulation and depletion). **f** Schematic illustrations of the reaction process for Ni_2P and Pt-Ni_2P catalysts. **g** Faradaic efficiency of NO_2^-. **h**. Free energy of the reaction pathway during UOR.

hydroxide surface layer is the real active species during UOR. Thereafter, the NiOOH (001) model was utilized to investigate the electrochemical conversion of urea. Differential charge density exhibited an electron depletion region around the Pt sites. The 'electron-donating' groups ($-NH_2$) in urea would be preferentially adsorbed on the positive region to accelerate the urea splitting process (Figure 3e).

As evidenced by in situ spectroscopic observations (Figure 3b), a stronger vibration peak of CNO^- species would signify that the C–N bond can be more readily cleaved on Pt-NiOOH (Figure 3f). It was suggested by previous studies that the "cyanate" pathway with over 50 % selectivity of NO_2^- was probably contributed by enriched NiOOH sites.[8] To verify the formation of NO_2^- during UOR, the electrolyte was collected and quantitatively determined by a Griess test.[34] The Faradaic efficiencies (FE) of NO_2^- for both Ni_2P and Pt–Ni_2P catalysts were all above 50 % and gradually enhanced as the applied potential increased. With Pt mediation, the highest FE_{NO2} could reach 74 ± 1 % (Figure 3g). The FE of N_2 and O_2 was also obtained (Supplementary Figure S15). The FE of N_2 and O_2 are less than 50 %, demonstrating the main products of nitrite. The FE_{NO2} at different times, including 0.5, 2.4, 10.0, and 23.0 h, respectively, were evaluated. With the increase in operating time, the FE_{NO2} exhibits a relatively stable selectivity (Supplementary Figure S16). The free energy of the reaction pathway during UOR was subsequently calculated (Figure 3h and Supplementary Figure S17). It was found that the rate-determining step was the C–N cleavage to form the intermediates of $*NH_2$ and CNO^- species and relatively lower free energy of 0.64 eV than that of NiOOH (1.48 eV) was found after incorporating Pt sites. This result strongly validates that the Pt sites could remarkably reduce the energy barrier to promote the the C–N cleavage during urea conversion.

Although some studies have been working on obviating the over-oxidation of N-products, complicated strategies with high costs are implemented to generate low-economic

N_2. In terms of the high value of nitrite in the areas of pharmaceuticals, agriculture, and food processing industries, direct utilization of urea-bearing wastewater to synthesize nitrite chemicals would be of great importance for the sustainable nitrogen economy, specifically when coupled with an anodic reaction like hydrogen production, NO_x electro-reduction, etc (Figure 4a).

To achieve this promising vision, the hydrogen evolution reaction (HER) performance of as-prepared Pt–Ni_2P catalysts was evaluated, which exhibits superior activities than commercial Pt/C catalysts and high stability at 100 mA cm^{-2} over 100 h (Supplementary Figure S18). As for the two-electrode system, the Pt–Ni_2P catalyst also shows outstanding activities compared to pure Ni_2P and has potential to replace OER in practical scenarios (Supplementary Figure S19). During 12 hours chronopotentiometry tests at 100 mA cm^{-2}, the cell voltage was stable without conspicuous increases. Moreover, the nitrite production rate could reach 0.82 mol kWh^{-1} cm^{-2} after introducing Pt sites (Figure 4c).

Another proof of concept for substituting OER with UOR in energy conversion systems is the zinc (Zn)-air battery. The cycling measurements over 66 hours were carried out with and without adding urea, labeled as Zn-air battery and Zn-urea-air battery. The charging process involving OER would proceed with UOR instead. The charging curves of the Zn-air battery and Zn-urea-air battery demonstrated a remarkable reduction of the charging voltage after adding urea to the electrolyte (Supplementary Figure S20). The cycling stability test during 66 h further exhibits about ~162 mV decrease in the charging voltage than that of the Zn-air battery (Figure 4d).

To realize urea-assisted hydrogen production for large-scale applications by direct usage of urea-bearing wastewater, the membrane electrode assembly (MEA) test was conducted (Figure 4e). Impressively, as-prepared Pt–Ni_2P catalysts possessed superior activity (Supplementary Figure S21) and stability at industrial-level current densities of 200 mA cm^{-2} during chronopotentiometry measurement over 135 h. No conspicuous voltage depletion could be

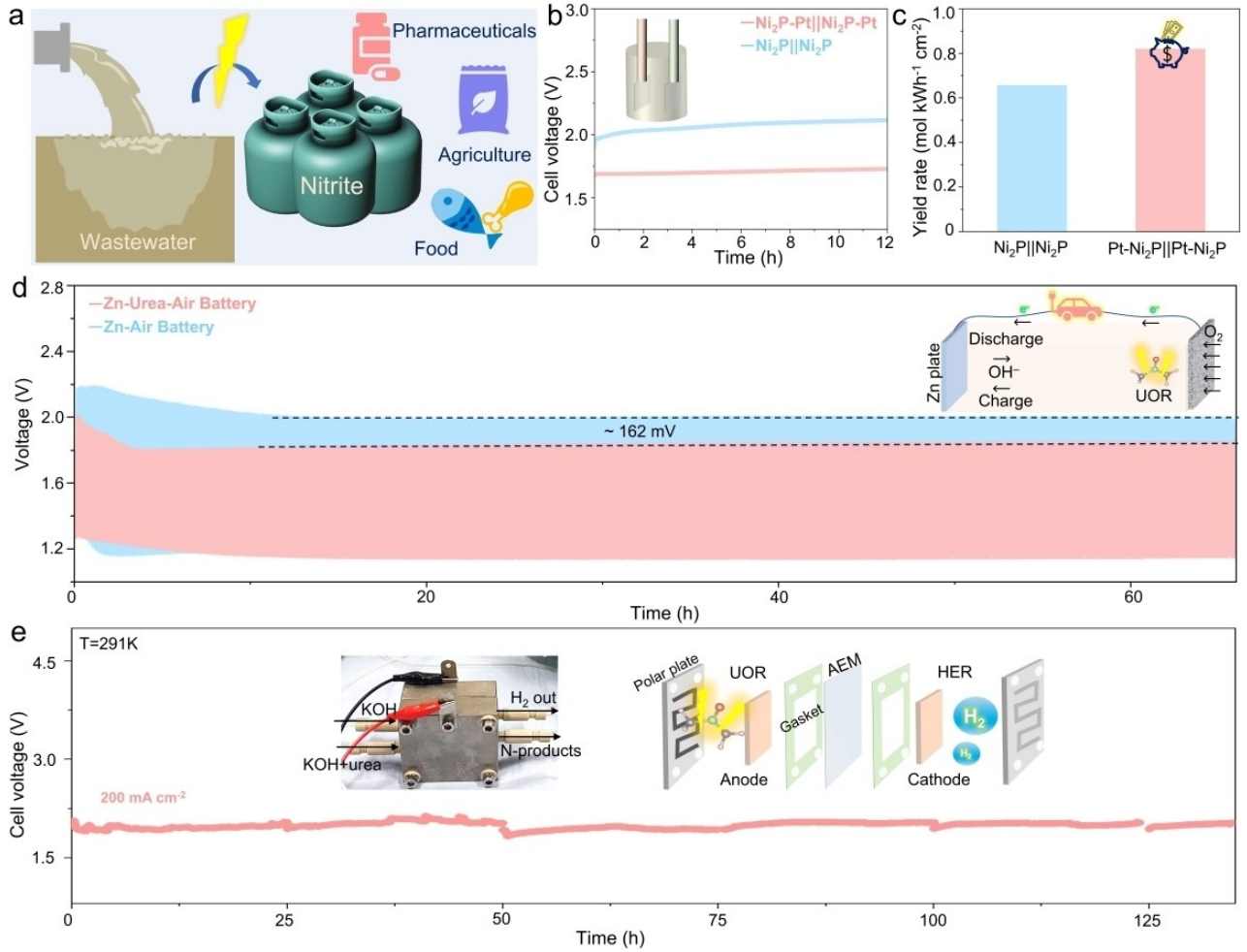

Figure 4. **Applicability verification. a** Schematic illustrations of nitrite direct production from urea-bearing wastewater. **b** stability test during 12 hours for nitrite production. **c**. Yield rate of nitrite. **d** Electrochemical measurement for Zn-air battery and Zn-urea-air battery (current density of 5 mA cm^{-2}); **e** Urea-assisted hydrogen production at current density of 200 mA cm^{-2} during MEA tests.

observed, implying the possibility for extensive practical applications.

Conclusion

In conclusion, the high activity, selectivity, and stability of nitrite production are achieved on Pt-mediated Ni_2P catalysts. By incorporating the low loading mass of Pt ($80\ \mu g\,cm^{-2}$), the Pt–Ni_2P catalysts exhibit superior UOR activity amidst the concurrent process of UOR and OER, while also showcasing exceptional nitrite selectivity among UOR product pathways. Specifically, promising direct nitrite production rate ($0.82\ mol\,kWh^{-1}\,cm^{-2}$), remarkable long-term durability tests of 60 h Zn-urea-air battery operation, and over 135 h nitrite and hydrogen production during MEA test demonstrate the practicality of Pt–Ni_2P catalysts. Integrating with in situ spectroscopic analysis and theoretical calculations, the Pt sites redistribute the charge density around Ni sites, lowering the energy barrier and proceeding with the cleavage of the C–N bond, which facilitated high-value nitrite production. Correspondingly, different from the majority of works on ameliorating the inevitable over-oxidation reaction to obtain low-value N_2 gas, we first suggested a close loop for the nitrogen cycle economy when coupled with other anodic reactions like NO_x electro-reduction. It is expected that this work supplies valuable insights into the regulation of electrocatalysts for green energy production.

Author Contributions

J. Z., I. P. P, and G. H. devised experiments; J. Z. synthesized the samples and performed all experimental studies; J. Z. and J. F. conducted computational calculations; G. H. and I. P. P. directed and supervised this project. J. Z. wrote the manuscript. J. Z., L. K., L. L, F. G., J. L., J. C., W. Z., M. L., R. C, and L.M. provided suggestions and guidance for this project.

Acknowledgements

The authors would like to thank the Open Foundation of the State Key Laboratory of Silicate Materials for Architectures at WUT (no. SYSJJ2020-04), the Engineering and Physical Sciences Research Council (EPSRC, EP/027433/3), the Cooperation project of Gansu Academy of Sciences (2020HZ-2) and UK Research and Innovation (UKRI) under the UK government's Horizon Europe funding (101077226; EP/Y008707/1). J. C. Z thanks the funding support from China Scholarship Council/University College London for the joint Ph.D. scholarships.

Conflict of Interest

The authors declare no conflict of interest.

Data Availability Statement

The data that support the findings of this study are available from the corresponding author upon reasonable request.

Keywords: Mediation engineering strategy · Urea oxidation reaction · Dynamic active sites · High-value products

[1] X. Zou, M. Tang, Q. Lu, Y. Wang, Z. Shao, L. An, *Energy Environ. Sci.* **2024**, *17*, 386–424.
[2] J. Li, H. Li, K. Fan, J. Y. Lee, W. Xie, M. Shao, *Chem Catal.* **2023**, *3*, 100638.
[3] X. Zhang, S. Feizpoor, M. Humayun, C. Wang, *Chem Catal.* **2023**, 100840.
[4] J. Mao, J. Iocozzia, J. Huang, K. Meng, Y. Lai, Z. Lin, *Energy Environ. Sci.* **2018**, *11*, 772–799.
[5] Y. Yan, R. Wang, Q. Zheng, J. Zhong, W. Hao, S. Yan, Z. Zou, *Nat. Commun.* **2023**, *14*, 7987.
[6] S. W. Tatarchuk, J. J. Medvedev, F. Li, Y. Tobolovskaya, A. Klinkova, *Angew. Chem.* **2022**, *134*, e202209839.
[7] V. M. Zemtsova, A. G. Oshchepkov, E. R. Savinova, *ACS Catal.* **2023**, *13*, 13466–13473.
[8] J. Li, J. Li, T. Liu, L. Chen, Y. Li, H. Wang, X. Chen, M. Gong, Z. Liu, X. Yang, *Angew. Chem.* **2021**, *133*, 26860–26866.
[9] J. John, D. R. MacFarlane, A. N. Simonov, *Nat. Catal.* **2023**, *6*, 1125–1130.
[10] H. Zhang, H. Wang, X. Cao, M. Chen, Y. Liu, Y. Zhou, M. Huang, L. Xia, Y. Wang, T. Li, D. Zheng, Y. Luo, S. Sun, X. Zhao, X. Sun, *Adv. Mater.* **2024**, 2312746.
[11] Y. Wang, C. Wang, M. Li, Y. Yu, B. Zhang, *Chem. Soc. Rev.* **2021**, *50*, 6720–6733.
[12] X. Gao, S. Zhang, P. Wang, M. Jaroniec, Y. Zheng, S.-Z. Qiao, *Chem. Soc. Rev.* **2024**, *53*, 1552–1591.
[13] X. Gao, X. Bai, P. Wang, Y. Jiao, K. Davey, Y. Zheng, S.-Z. Qiao, *Nat. Commun.* **2023**, *14*, 5842.
[14] X. Xu, Y. Lu, J. Shi, X. Hao, Z. Ma, K. Yang, T. Zhang, C. Li, D. Zhang, X. Huang, Y. He, *Nat. Commun.* **2023**, *14*, 7708.
[15] Y.-N. Zhou, F.-T. Li, B. Dong, Y.-M. Chai, *Energy Environ. Sci.* **2024**, 10.1039.D3EE02627B.
[16] Z. Yang, S. Wang, C. Wei, L. Chen, Z. Xue, T. Mu, *Energy Environ. Sci.* **2024**, *17*, 1603–1611.
[17] R. Lin, L. Kang, T. Zhao, J. Feng, V. Celorrio, G. Zhang, G. Cibin, A. Kucernak, D. J. L. Brett, F. Corà, I. P. Parkin, G. He, *Energy Environ. Sci.* **2022**, *15*, 2386–2396.
[18] J. Zhang, J. Zhu, L. Kang, Q. Zhang, L. Liu, F. Guo, K. Li, J. Feng, L. Xia, L. Lv, W. Zong, P. R. Shearing, D. J. L. Brett, I. P. Parkin, X. Song, L. Mai, G. He, *Energy Environ. Sci.* **2023**, *16*, 6015–6025.
[19] M. Zhong, M. Xu, S. Ren, W. Li, C. Wang, M. Gao, X. Lu, *Energy Environ. Sci.* **2024**, *17*, 1984–1996.
[20] S. Xu, X. Ruan, M. Ganesan, J. Wu, S. K. Ravi, X. Cui, *Adv. Funct. Mater.* **2024**, 2313309.
[21] Z. Ji, W. Yuan, S. Zhao, T. Wang, S. Umer, S. Ding, J. Liu, J. Liu, Y. Zhao, W. Hu, *Chem Catal.* **2023**, *3*, 100501.
[22] J. Zhu, L. Xia, R. Yu, R. Lu, J. Li, R. He, Y. Wu, W. Zhang, X. Hong, W. Chen, Y. Zhao, L. Zhou, L. Mai, Z. Wang, *J. Am. Chem. Soc.* **2022**, *144*, 15529–15538.
[23] Y. Peng, X. Wang, C. Wang, W. Bi, Q. Jiang, Z. Tian, *Chem Catal.* **2023**, *3*, 100505.
[24] B. Zhou, Y. Li, Y. Zou, W. Chen, W. Zhou, M. Song, Y. Wu, Y. Lu, J. Liu, Y. Wang, S. Wang, *Angew. Chem. Int. Ed.* **2021**, *60*, 22908–22914.
[25] W. Chen, C. Xie, Y. Wang, Y. Zou, C.-L. Dong, Y.-C. Huang, Z. Xiao, Z. Wei, S. Du, C. Chen, B. Zhou, J. Ma, S. Wang, *Chem* **2020**, *6*, 2974–2993.

[26] W. Chen, L. Xu, X. Zhu, Y. Huang, W. Zhou, D. Wang, Y. Zhou, S. Du, Q. Li, C. Xie, L. Tao, C. Dong, J. Liu, Y. Wang, R. Chen, H. Su, C. Chen, Y. Zou, Y. Li, Q. Liu, S. Wang, *Angew. Chem. Int. Ed.* **2021**, *60*, 7297–7307.
[27] M. Alnot, V. Gorodetskii, A. Cassuto, J. J. Ehrhardt, *Thin Solid Films* **1987**, *151*, 251–262.
[28] J. D. Rogers, V. S. Sundaram, G. G. Kleiman, S. G. C. Castro, R. A. Douglas, A. C. Peterlevitz, *J. Phys. F Met. Phys.* **1982**, *12*, 2097–2102.
[29] Y. Liao, Y. Chen, L. Li, S. Luo, Y. Qing, C. Tian, H. Xu, J. Zhang, Y. Wu, *Adv. Funct. Mater.* **2023**, *33*, 2303300.
[30] A. S. Rasal, H. M. Chen, W.-Y. Yu, *Nano Energy* **2024**, *121*, 109183.
[31] Y. Pan, D. Mei, C. Liu, Q. Ge, *J. Phys. Chem. C* **2011**, *115*, 10140–10146.
[32] L. Wang, S. Zhu, N. Marinkovic, S. Kattel, M. Shao, B. Yang, J. G. Chen, *Appl. Catal. B* **2018**, *232*, 365–370.
[33] S. Sun, X. Zhou, B. Cong, W. Hong, G. Chen, *ACS Catal.* **2020**, *10*, 9086–9097.
[34] X. Li, P. Shen, X. Li, D. Ma, K. Chu, *ACS Nano* **2023**, *17*, 1081–1090.

Manuscript received: April 13, 2024
Accepted manuscript online: June 13, 2024
Version of record online: ■■, ■■

Research Article

Urea Oxidation

J. Zhang, J. Feng, J. Zhu, L. Kang, L. Liu, F. Guo, J. Li, K. Li, J. Chen, W. Zong, M. Liu, R. Chen, I. P. Parkin,* L. Mai,* G. He* _____ **e202407038**

Regulating Reconstruction-Engineered Active Sites for Accelerated Electrocatalytic Conversion of Urea

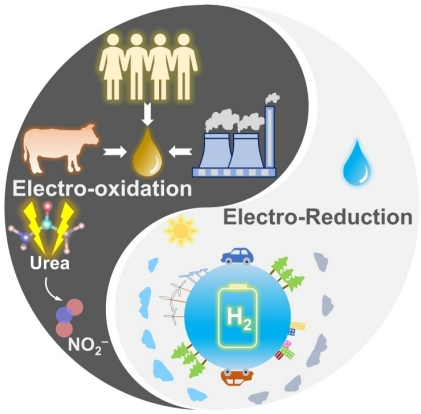

Developing highly efficient electrocatalysts for urea oxidation reaction (UOR) to achieve nitrogen cycle with high value-added products.